Solid State Ionics 341 (2019) 115045

Contents lists available at ScienceDirect

Solid State Ionics

journal homepage: www.elsevier.com/locate/ssi

Effects of anodic layer thickness on overall performance of all-solid-state electrochromic device

Gamze Atak, Özlem Duyar Coşkun*

Hacettepe University, Department of Physics Engineering, Thin Film Preparation and Characterization Laboratory, 06800 Beytepe, Ankara, Turkey

ARTICLE INFO

Keywords:
All-solid-state electrochromic device
NiO film
Electrochromism
Magnetron sputtering
Optical modulation
Coloration efficiency

ABSTRACT

In the present study, the effects of the anodic electrochromic layer employed in the all-solid-state ECD in the structure of ITO/NiO/Ta_2O_5/WO_3/ITO/glass on the optical and electrochromic performances of the device are investigated. For this purposes, the nickel oxide films with various thicknesses were deposited onto glass and ITO-coated glass substrates by RF magnetron sputtering technique using a NiO target in pure Ar atmosphere at room temperature. The optical, structural and electrochromic properties of the NiO films with various thicknesses (140 nm, 230 nm, 310 nm and 480 nm) were investigated. The optical transmission of the films decreased as the thickness of the films increased. The X-ray diffraction patterns showed that the films were polycrystalline phase and the peak density increased with the film thickness. The optical band gap was found to decrease from 3.71 to 3.50 eV with increasing film thickness. The root-mean-square (rms) surface roughnesses of the films increased (from 1.43 nm to 2.94 nm) with increased film thickness. Coloration efficiencies and optical modulations of the NiO films were obtained for a wide spectral range. The amount of inserted/extracted charges into/from the films during bleaching/coloring were obtained as a function of the film thickness. The highest coloration efficiency (40.7 cm^2/C) and optical modulation (27.8%) at a wavelength of 550 nm were obtained for the NiO film with a thickness of 480 nm. Finally, all-solid-state electrochromic devices were fabricated by using the thinnest and thickest NiO films with a configuration of ITO/NiO/Ta_2O_5/WO_3/ITO/glass. The ECD-1 device with a thinner NiO layer showed a high optical modulation (36.4%). On the other hand, the ECD-2 with a thicker NiO layer showed a very low optical modulation (1.5%) at 550 nm. Our results indicated that the thicker NiO film exhibited better electrochromic properties in the half-cell configuration, while the thinner one showed higher optical modulation in electrochromic device fabrication with a complete-cell configuration. Therefore, the effect of the thickness of a NiO layer on the electrochromic performance of both the half-cell and complete cell configuration electrochromic coatings were investigated in detail.

1. Introduction

Nickel oxide (NiO) is a transition metal oxide, which has a wide band gap and shows p type semiconductor characteristics. NiO is a promising material for applications in electrochromic devices, p-type transparent conductive films and gas sensors due to its low cost, chemical stability and unique electrical and optical properties [1–4].

Optical properties of electrochromic (EC) materials such as transmission, absorption and reflection can be reversibly changed when an external potential difference is applied to them. Electrochromic materials and devices have been developed as an alternative technology for light and heat management. Nickel oxide films are one of the most promising anodic electrochromic materials, which are colored via ion extraction from the film surface during the electrochromic cycle. WO_3 and NiO are widely used as an active and a counter electrochromic layer in a full device configuration, respectively. WO_3 and NiO can be colored and bleached instantaneously under the applied voltage to the device. Thus the overall optical modulation increases than those obtained in the half-cell configuration for each individual layer of film.

NiO films change their color reversibly from transparent to brown by electrochemical cycling in an electrolyte solution (e.g. $LiClO_4$/PC). Electrochromic reaction of nickel oxide thin film exhibits a two-stage reaction mechanism in Li^+ containing electrolytes [4]:

$$NiO_x + yLi^+ + ye^- \rightarrow Li_yNiO_x \quad (1)$$

$$Li_yNiO_x \overset{\text{colored}}{\underset{\text{tranparent}}{\Leftrightarrow}} Li_{y-z}NiO_x + zLi^+ + ze^- \quad (2)$$

NiO films have valuable characteristic EC properties such as higher

* Corresponding author.
E-mail addresses: gbaser@hacettepe.edu.tr (G. Atak), duyar@hacettepe.edu.tr (Ö.D. Coşkun).

https://doi.org/10.1016/j.ssi.2019.115045
Received 19 February 2019; Received in revised form 27 June 2019; Accepted 10 August 2019
Available online 20 August 2019

coloration efficiency and good durability during EC cycles [4]. However, their electrochromic properties have not been fully understood yet. Since these films are widely used in EC applications, there are many ongoing researches on NiO films.

Nickel oxide films have been deposited by using different techniques such as sputtering [5–9], electron beam evaporation [10], chemical vapor deposition [11] and sol-gel [12]. Among these, sputtering technique is widely used due to its high growth rate capability, applicability to large areas and easy control over the composition of deposited films [13–16]. Properties of the deposited films mainly depend on the deposition parameters such as working pressure, sputtering power, substrate temperature and oxygen partial pressure. It is evident that optical, structural and electrochromic properties can be improved by optimization of the preparation conditions. There is a very limited literature related with the effects of thickness of an electrochromic layer on device output [17,18]. However, the thickness of electrochromic layer is one of the main parameters of half-cell and full-cell electrochromic device performance.

In this study, the variations in the optical, structural and electrochromic properties of the NiO films with various thicknesses deposited by RF sputtering technique were investigated in detail. Finally, all-solid-state electrochromic devices with a configuration of ITO/NiO/Ta_2O_5/WO_3/ITO/glass were fabricated in which various thicknesses of NiO films used to understand the effect of the thickness of an anodic layer used in it.

2. Experimental studies

The NiO films were deposited on glass substrates by using a Nanovak RF magnetron sputtering system at room temperature. The deposition chamber was evacuated to a base pressure of 2.8×10^{-6} Torr. The NiO target (99.9% in purity) was 2″ in diameter and 1/4″ in thickness. The deposition was performed in an Ar plasma without a reactive gas. The distance between the target and the substrate was 7 cm. The sputtering pressure and power was maintained at 35 mTorr and 75 W, respectively. Homogeneity of the films was provided by rotating the substrate holder at a constant speed during the deposition process. The deposition was started by opening the shutter between the target and the substrate holder following 10 min of pre-sputtering process.

The NiO films were also deposited on ITO coated glass substrates in order to perform the electrochemical measurements. The ITO thin films with a thickness of 165 nm were deposited by using RF magnetron sputtering technique. The deposition was performed at 36 mTorr Ar plasma by using an ITO target at 200 °C. The sputtering power was maintained at 50 W. Their sheet resistance was 125 Ω/□. The average optical transmission of the films was about 82% in the visible spectrum.

Finally, the unique design all-solid-state electrochromic devices with various thicknesses of NiO were fabricated by using RF magnetron sputtering technique. The main configuration of the devices was ITO/NiO/Ta_2O_5/WO_3/ITO/glass.

The optical transmission and reflection measurements of the films were performed using an Aquila nkd-8000e spectrophotometer over the wavelength range of 350–1100 nm. The film thicknesses were measured by using a quartz crystal monitor during the deposition process.

The crystallographic structures of the films were investigated by using a Rigaku Ultima-IV X-ray diffractometer with Cu K_α radiation ($\lambda = 0.15418$ nm). The surface morphologies of the films were investigated by a XE-100E Park System atomic force microscope (AFM).

In order to investigate electrochromic properties of the structures in both half-cell and full-cell configuration, a CHI 600C model electrochemical analyzer and a conventional three-electrode cell were used. An $Ag/AgCl_{KOH}$ and a platinum wire were used as a reference electrode and a counter-electrode, respectively. A 0.01 M solution of $LiClO_4$ in propylene carbonate (PC) was used as an electrolyte. The cyclic voltammetry (CV) measurements of the films were performed with a scan rate of 50 mV/s over the voltage range of ± 2 V. The corresponding chronoamperometry (CA) measurements of the films were performed by applying +2 V and −2 V with a duration of 20 s.

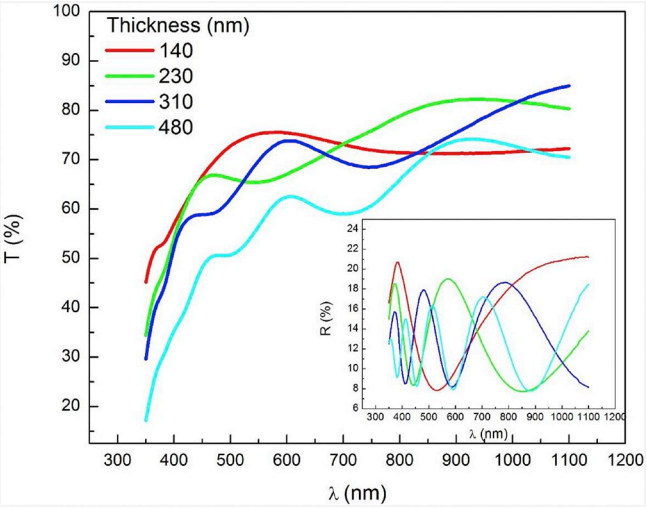

Fig. 1. The optical transmission and reflection spectra of the NiO films deposited on glass substrates with various thicknesses.

The optical absorbance spectra of both the bleached and colored states of the films were measured by using a Hitachi U0080D diode array spectrophotometer over the spectral range of 190–1100 nm at normal incidence during the EC cycles.

The electrochemical impedance spectroscopy (EIS) was used to understand the kinetics of electrochemical reactions at the electrodes. The electrochemical impedance measurements of the NiO films were performed at 0.05 V over a frequency range of 0.01 Hz–0.2 MHz using a three-electrode cell.

3. Results and discussion

3.1. Optical and structural properties of the NiO films

The optical transmission and reflection spectra of the NiO films deposited with various thicknesses (140 nm, 230 nm, 310 nm and 480 nm) were shown in Fig. 1, respectively. The figure clearly indicates that the optical transmission of the film decreased as thickness of the film increased. The optical transmission of the films decreased from 75.2% to 56.5% at 550 nm when the film thickness increased from 140 nm to 480 nm as seen in the figure. The optical transmission of the films is expected to depend on the film properties such as oxygen deficiencies, impurity centers, grain sizes, structural homogeneity, and level of crystallinity [19,20]. A lower optical transmission for the thicker films may be related with higher surface light scattering due to increase in surface roughness [16].

The optical transmission and reflection measurement were used to calculate the optical losses which include absorptions and scatterings (Optical loss = 1-T-R). Fig. 2 shows the optical losses of the NiO films. It is clear that the thicker NiO film has the highest optical losses. The optical losses of the films can be originated from the absorption and the scatterings from grain boundaries, voids, surface roughness or microcracks [21].

Fig. 3 shows the optical absorbance spectra of the films with various thicknesses. The optical absorbance spectra of the films were used to determine the optical band gap by Tauc formula given in Eq. (3):

$$\alpha_{h\nu} = A\,(h\nu - E_g)^r \tag{3}$$

where α is absorption coefficient, A is band edge constant, hυ is photon energy, E_g is optical band gap, and r is power which takes values of 1/2, 3/2, 2 and 3 for direct allowed, direct forbidden, indirect allowed and

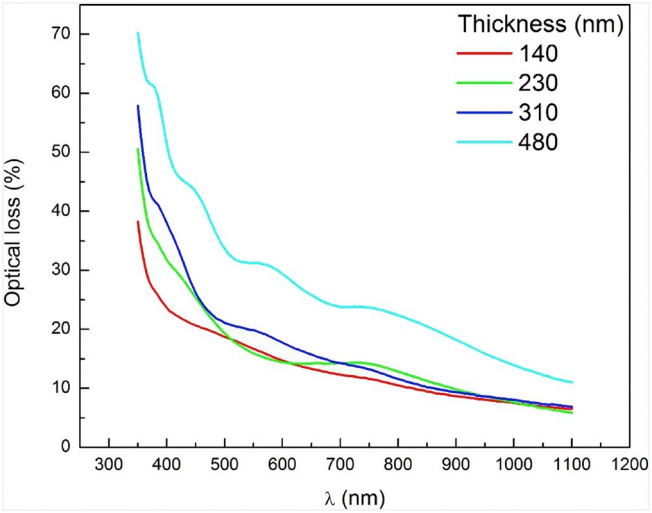

Fig. 2. The optical loss spectra of the NiO films with various thicknesses.

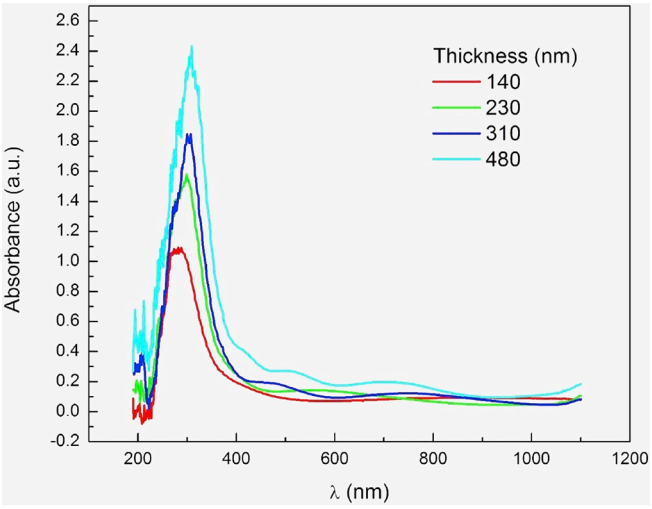

Fig. 3. The optical absorbance spectra of the films with various thicknesses.

indirect forbidden transitions, respectively [22,23]. r = 1/2 is chosen due to the direct allowed transition of NiO. $(\alpha h\nu)^2$ versus hν plot, called Tauc plot, has a linear region with slope A^2 and whose extrapolation to $\alpha(h\nu) = 0$ gives value of E_g. The optical band gap of the film decreased from 3.71 eV to 3.50 eV with increased film thickness. This can be attributed to the improvement in crystallinity, morphological changes of the films, structural defects in the films, changes in atomic distances and grain size [24,25]. Similar band gap narrowing effect has been reported by many other researchers and this effect is attributed to the increase in absorbance for thicker films in which large numbers of atoms available to absorb incident photon energy [26–29].

Determination of spectral optical constants are crucial to understand optical characteristics of materials. The complex refractive index is denoted by n* (n* = n + ik where, n is a real part called as a refractive index, and k is an imaginary part called as an extinction coefficient, respectively). Extinction coefficient is related with total optical losses caused by both absorption and scattering. For an ideal transparent material, k should be zero in visible and infrared region, as the films do not absorb light. However, NiO films are semi-transparent hence; they have relatively higher k compared to the highly transparent ones [30]. The wavelength dependence of refractive index n(λ), extinction coefficient k(λ) and the thickness of the films were determined by fitting the transmission and reflection spectra simultaneously, using Harmonic Oscillator Model. The measured and calculated (fitted) transmission and reflection curves of NiO films with respect to the wavelength are shown in Fig. 4.

Fig. 5 illustrates the estimated refractive index as a function of wavelength for the films with various thicknesses. The inset of the figure also shows the extinction coefficient of those films as a function of wavelength. It is seen that the films have higher extinction coefficients in the order of 10^{-2} that is also the indication of the observed higher absorption of the films.

The AFM images and X-ray diffraction patterns were analyzed to investigate the structural properties of the NiO films with different thicknesses. The root-mean-square (rms) values of the surface roughness of the films increased (from 1.43 nm to 2.94 nm) with increased film thickness. Surface roughness strongly effects the optical, electrical and mechanical properties of the films. Surface roughness is an important parameter to understand the light scattering at the film surface. The increase in surface roughness of the film causes the increased light scattering reducing the optical transmission of the film. The decrease in the optical transmission of the film can be also attributed to the increase in crystallinity of films, which results in the higher scattering of light [25,31,32].

The estimated optical band gap (E_g), refractive indices (n) by fitting process and rms surface roughnesses (R_{rms}) of each film were given in Table 1.

The X-ray diffraction patterns of the films were shown in Fig. 4. In the figure, two basic diffraction peaks ((111) 2θ = 37.7°, (200) 2θ = 42.7°, JCPDS 79-0423) from the planes of the cubic structure of NiO were observed with a higher intensity [33]. The substrate temperature increased from 25 °C up to 67 °C as the growth time increased up to 210 min. So the increase in the crystallinity with the increased film thickness could be attributed to the plasma heating effect during the deposition [34]. It was found that the plasma heating effect was an important factor for the crystallinity of the films even there is no substrate heating. In the literature, the effects of the film thickness on the diffraction intensity was explained by Chen et al. [9]. As the film thickness increased, the diffraction intensity increased due to the more crystallites grown in the structure. The average crystallite size (*D*) is determined from the full width at the half maximum (FMHM) of the XRD peaks using the Debye-Scherrer equation:

$$D = \frac{\kappa \lambda}{\beta \cos\theta} \quad (4)$$

where κ is the shape factor with a typical value of 0.9, λ is the wavelength of the incident beam, β is the full width at the half maximum of the XRD peak corresponding to the diffraction angle θ. As seen in the Fig. 6, the (200) peak has the highest intensity indicating that (200) is the preferred orientation of the films. The (200) peak was used to calculate the average crystallite sizes. The estimated values of the average crystallite size were given in Table 2. It is observed that the crystallite size increased with increased film thickness. As the film thickness increases the (200) peak becomes narrower suggesting that the increase in thickness leads to an increase in grain size. The crystallite size of the thinner NiO film was estimated to be 10.72 nm, which was 14.42 nm for the thicker NiO film. The increase in grain size with increasing film thickness is an indication of the improved crystallization degree of the film [35]. Corresponding lattice constants of these samples were calculated as 3.60 Å and 3.59 Å, respectively.

3.2. Electrochromic and electrochemical properties of the NiO films

The three main parameters are generally used to characterize EC performances of materials: optical modulation (ΔT), optical density (ΔOD) and coloration efficiency (CE). Optical modulation is the difference between the transmission in bleached and colored state at a specific wavelength. Coloration efficiency is the ratio of change in optical density (ΔOD) at a specific wavelength to the amount of charge inserted into/extracted from unit area of the film:

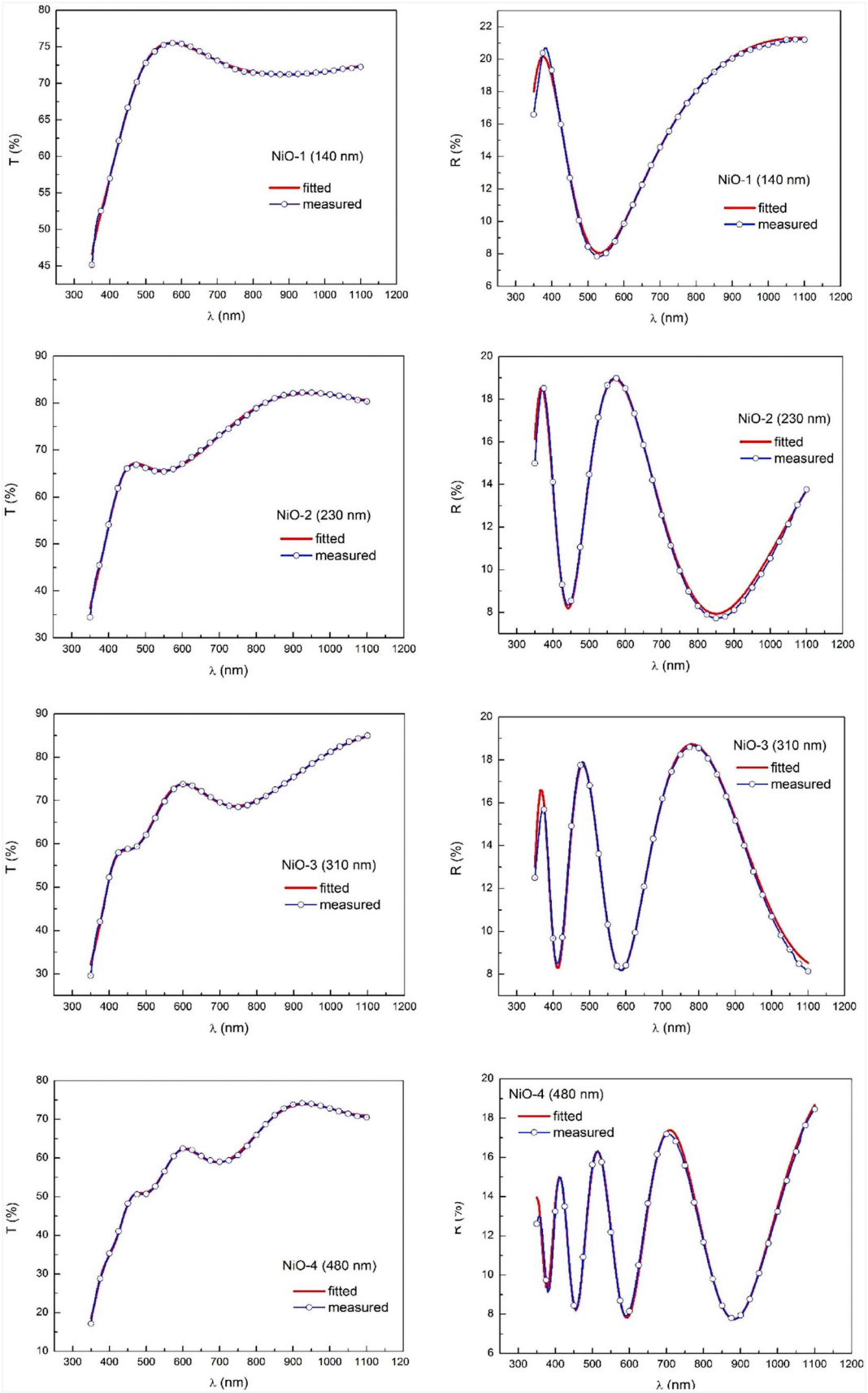

Fig. 4. The measured and calculated transmission and reflection curves of NiO films with respect to wavelength.

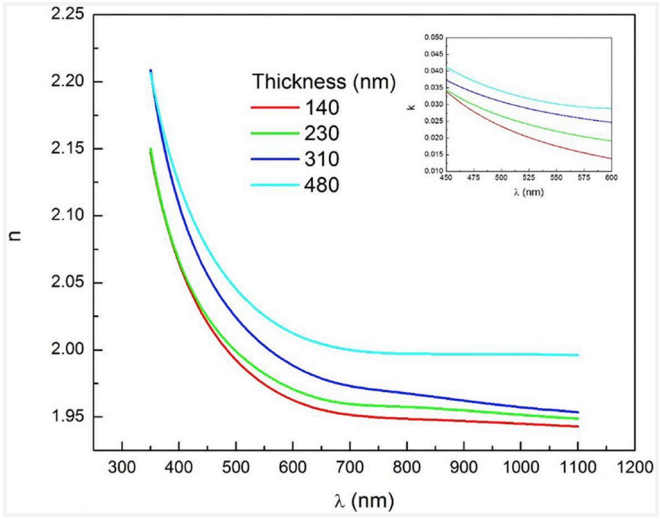

Fig. 5. The variation of refractive index (n) with NiO film thicknesses. Inset shows the wavelength dependence of extinction coefficient of those films.

Table 1
The optical band gap (E_g), refractive index (n) and rms surface roughness (R_{rms}) of each film.

Film	d (nm)	$n_{\lambda=550\ nm}$	E_g (eV)	R_{rms} (nm)
NiO-1	140	1.97	3.71	1.43
NiO-2	230	1.98	3.62	2.03
NiO-3	310	2.00	3.60	2.19
NiO-4	480	2.03	3.50	2.94

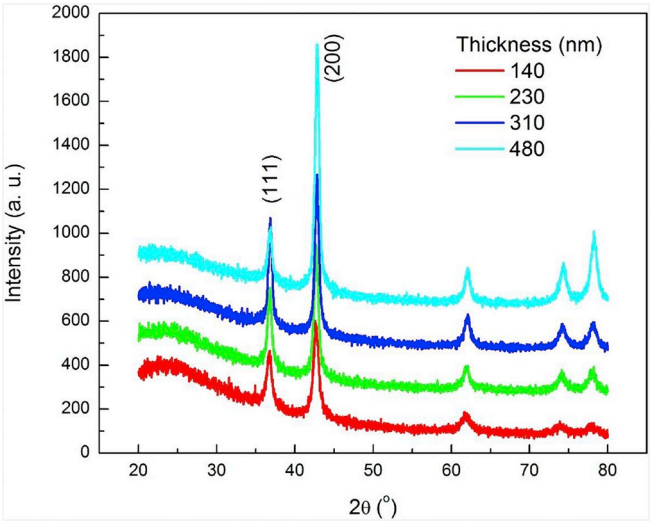

Fig. 6. The XRD patterns of the NiO films with various thicknesses.

Table 2
Structural parameters of the NiO films with various thicknesses obtained from XRD patterns.

Film	FWHM (°)	2Θ (°)	Crystallite size (D) (nm)	Lattice constant (Å)	Unit cell volume (Å^3)
NiO-1	0.796	42.672	10.72	3.599	46.6
NiO-2	0.660	42.707	12.92	3.596	46.5
NiO-3	0.610	42.769	13.99	3.588	46.2
NiO-4	0.592	42.825	14.42	3.593	46.4

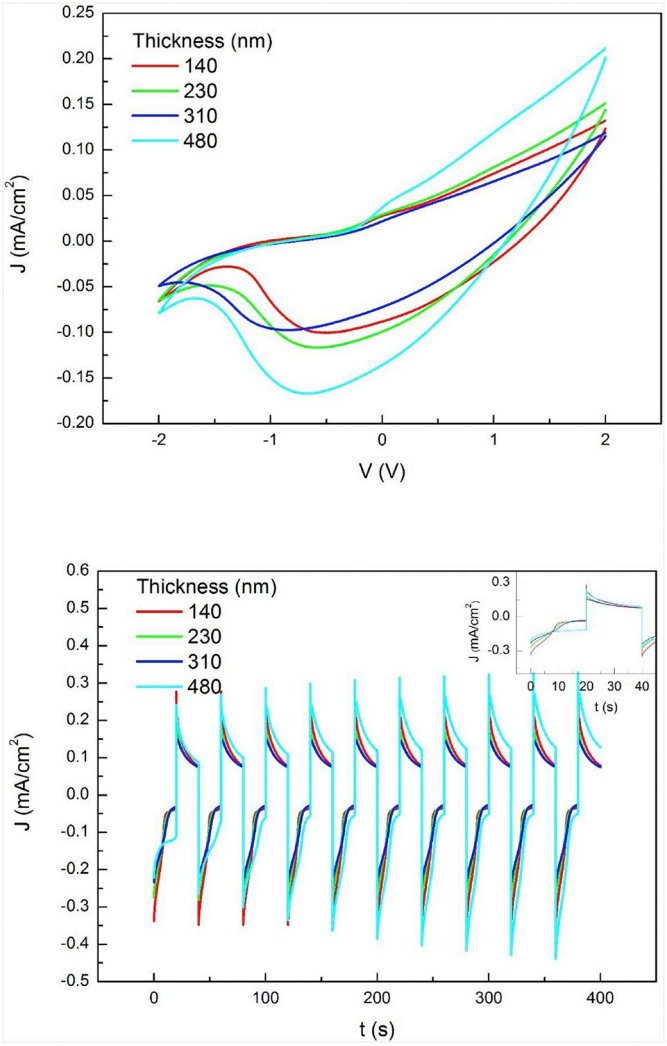

Fig. 7. The cyclic voltammetry and chronoamperometry curves of the NiO films with various thicknesses.

$$\Delta T = T_b - T_c \quad (5)$$

$$\Delta OD = \log\left(\frac{T_b}{T_c}\right) \quad (6)$$

$$CE = \Delta OD/\Delta Q \quad (7)$$

where T_b and T_c are the bleached and colored state transmissions of the films at a specific wavelength, respectively [33,36].

Fig. 7 shows the cyclic voltammetry (CV) and chronoamperometry (CA) curves at the end of 20th cycle of the NiO films with various thicknesses, respectively. The NiO films deposited on ITO coated glass were used as a working electrode in a three-electrode cell to perform CV and CA measurements. The areas of the curves cyclic voltammetry increased with increased film thickness that is the indication of the increasing charge storage capacity of the NiO film with the increase in film thickness.

The cathodic and anodic charges were calculated by integrating the corresponding region of the CV curves. The total injected charge into the film (ΔQ_C) and the total extracted charge from the film (ΔQ_A) were obtained by integrating the area under the CA curves. The coloration efficiencies (CE) of the films were calculated by using ΔQ_A values for the NiO films due to their anodic coloration. Q_C, Q_A, I_C, I_A, ΔQ_C and ΔQ_A values were listed in Table 3.

Spectral coloration efficiencies and spectral optical modulations of the NiO films were seen in Fig. 8 and Fig. 9, respectively. The highest

Table 3
The electrochromic parameters of the NiO films with various thicknesses.

Film	d (nm)	Q_C (mC/cm^2)	Q_A (mC/cm^2)	I_C (mA/cm^2)	I_A (mA/cm^2)	ΔQ_C (mC/cm^2)	ΔQ_A (mC/cm^2)
NiO-1	140	2.398	3.492	−0.037	0.076	3.866	−3.770
NiO-2	230	2.397	4.171	−0.031	0.074	4.194	−4.066
NiO-3	310	1.779	3.480	−0.030	0.076	3.276	−3.155
NiO-4	480	1.943	3.869	−0.111	0.088	4.076	−3.418

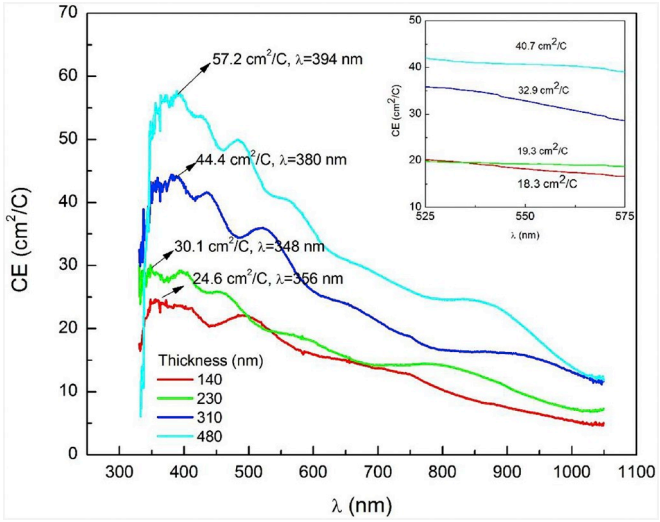

Fig. 8. The coloration efficiency spectra of the NiO films with various thicknesses.

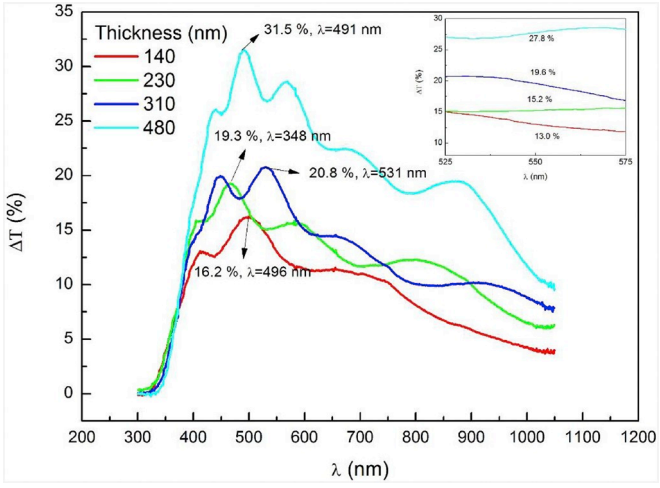

Fig. 9. The optical modulation spectra of the NiO films with various thicknesses.

CE and ΔT values and corresponding wavelength values were marked on the figures. The coloration efficiency and the optical modulation of the films improved with an increase in film thickness. The highest values of coloration efficiency and optical modulation were observed at the ultraviolet and the beginning of the visible regions. Both coloration efficiency and optical modulation were found to be lower in the infrared region. The highest coloration efficiency and optical modulation were obtained for the film with a thickness of 480 nm. The highest coloration efficiency of the film was 57.2 cm^2/C at 394 nm. The highest optical modulation of the film was 31.5% at 491 nm.

The bleached state and colored state optical transmission spectra of the NiO films with various thicknesses were shown in Fig. 10.

A rough surface along the grain boundaries is one of the key parameters for electrochromic activity that is more pronounced as the grain size increases, which can be beneficial for the ion insertion/extraction [37]. A rough surface allows easier diffusion of ions and provides larger surface area for charge-transfer reactions. The improvement in the electrochromic activity of the porous inorganic oxides has been reported in the literature [4,38]. In the present work, the surface roughness of the films increased with increased film thickness. It is observed that the ion insertion/extraction mechanism became more difficult at the smoother surfaces compared to the rougher surfaces.

Electrochromic behavior of the metal-oxide EC layers generally shows an improvement with increasing film thickness. As the film thickness increases, depth of diffusion also increases. Thus, the amount of charges contributing to electrochromic activity become dependent on the thickness of the film during the EC cycling [37]. Li^+ diffusion coefficient limits its intercalation/deintercalation properties in NiO films. Diffusion constants of the films for the Li^+ ions ($D_{Li}{}^+$) are calculated by using Randles-Sevcik equation given in Eq. (8):

$$i_{pa} = 0.4463\, n\, F\, C\, A \sqrt{\frac{n\, F\, \upsilon\, D}{R\, T}} \tag{8}$$

where I_{pa} is anodic peak potential, n is number of electrons involved in the reaction of the redox couple, F is Faraday's constant (96,485.33 C/mol), C is concentration of the electrolyte (mol/cm^3), A is area of working electrode (cm^2), ν is swept rate of potential (V/s), D is diffusion coefficient (cm^2/s), R is universal gas constant (8.314 J/mol·K) and T is absolute temperature (K) [39]. It is observed that the diffusion constants of the NiO films for the Li^+ ions ($D_{Li}{}^+$) increased from 1.37×10^{-13} to 1.36×10^{-10} cm^2/s with increased film thickness. The diffusion coefficient was reported to be between 1×10^{-10} to 1×10^{-14} cm^2/C in the literature [40,41].

The Nyquist plots for the NiO films deposited on ITO coated glass substrates were shown in Fig. 11. The equivalent circuit used to analyze the impedance curves was inserted in figure. The Nyquist plots for the films showed a semicircle in the high frequency region, which can be ascribed to the mass-transfer of the electroactive ionic species such as Li^+ within the electrolyte and to a vertical linear spike in the low frequency region, which indicates the diffusion-controlled transfer of the electroactive ionic species within this region [42]. A smaller semicircle means a lower charge-transfer resistance, whereas a lower slope implies a higher diffusion rate [43]. The film with a thickness of 140 nm and 480 nm thick films have the lowest charge-transfer resistance and the highest diffusion rate, respectively. When the diffusion rate increased, the electrochromic efficiency of the films (e.g. coloration efficiency and optical modulation) also increased. The resistance of electrolyte solution, which is also called as ohmic resistance (R_0), is independent of the films properties and its value equals to the high frequency intercept of the semicircle on the real impedance axis. In other words, the value of R_0 (550 Ω) can be observed at the starting point on the Nyquist plot. The resistance between ITO and NiO is called the contact resistance (R_1). Lower R_1 value was observed for the sample with a thickness of 480 nm. R_2 represents a charge transfer resistance, while CPE is a constant phase element.

The ionic conductivity of the film can be calculated by the following equation (Eq. 9):

$$\sigma_i = \frac{1}{R_b}\frac{d}{A} \tag{9}$$

where σ_i is ionic conductivity, d is film thickness, A is area of the film and R_b is bulk resistance of the film [44]. The highest ionic conductivity was obtained as 6.05×10^{-9} S/cm for the 480 nm thick NiO film.

3.3. Characterization of the all-solid-state electrochromic devices

The thinnest and thickest NiO films were used to fabricate the all-solid-state electrochromic devices (ECDs). The ECDs assembled by

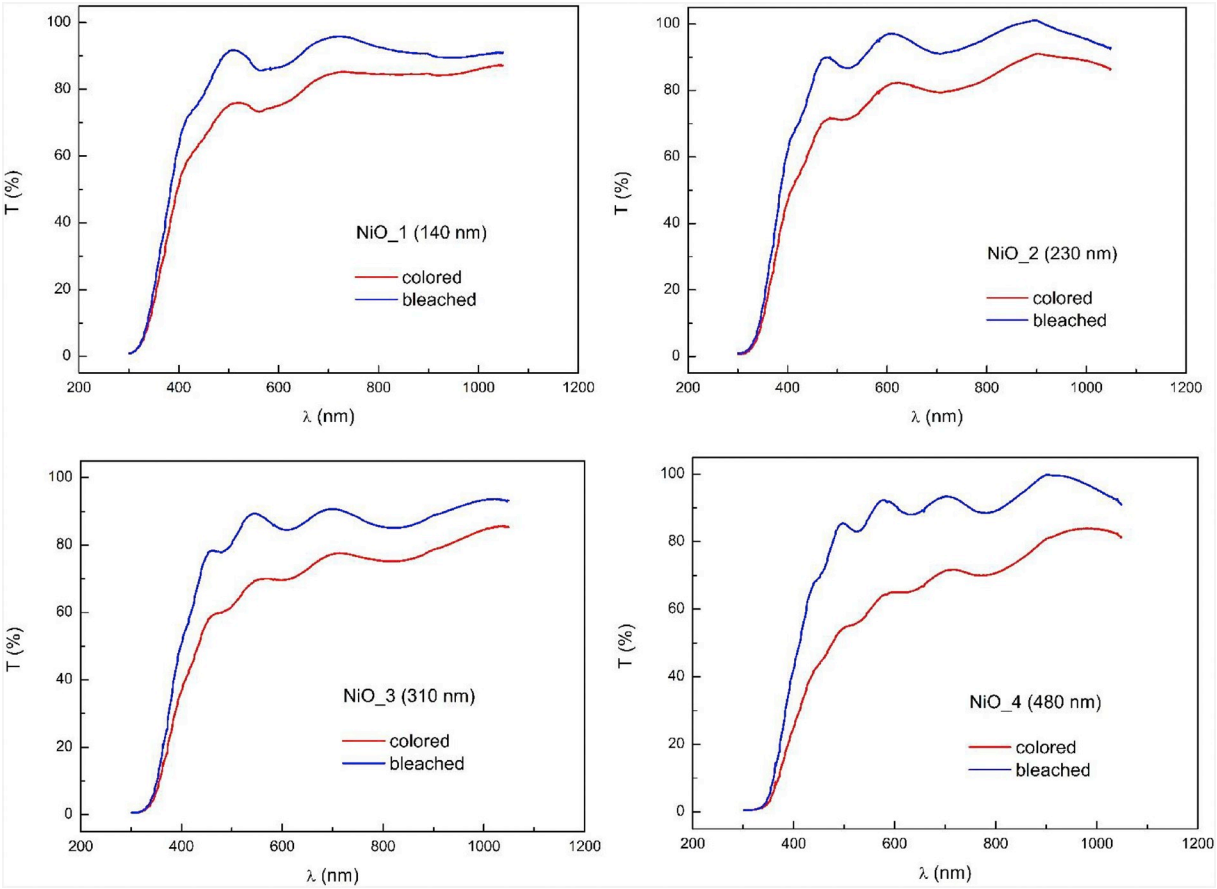

Fig. 10. The optical transmission spectra for the bleached state and colored state of the NiO films with various thicknesses.

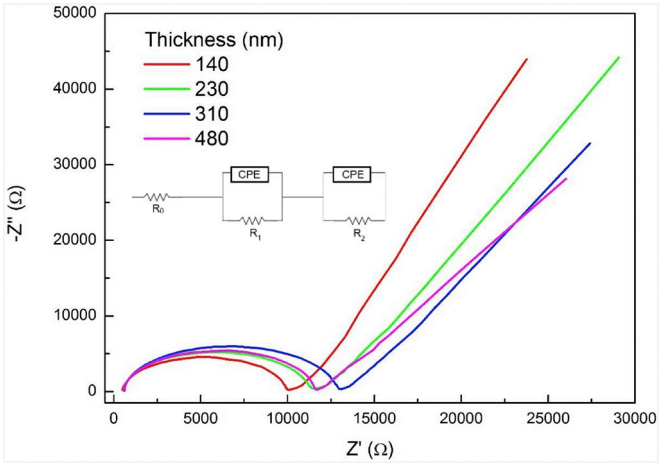

Fig. 11. The electrochemical impedance spectra of the NiO films with various thicknesses.

using NiO film with thickness of 140 nm and 480 nm were called as ECD-1 and ECD-2, respectively. The films used in the device fabrication were deposited by RF magnetron sputtering technique. The all-solid-state electrochromic devices were fabricated with a configuration of ITO/NiO/Ta_2O_5/WO_3/ITO/glass. In the device, ITO film acted as a transparent electrode, while the NiO film was used as an anodic electrochromic layer, Ta_2O_5 film as an ion conducting layer and WO_3 film as a cathodic electrochromic layer. Firstly, the WO_3 film was deposited onto the ITO coated glass substrates at room temperature by using a tungsten (W) target. The deposition process was performed in a plasma consisting of Ar (87.5%) and O_2 (12.5%) mixture. The sputtering power

Table 4
Detailed deposition parameters of the ECDs.

Target	Working pressure (mTorr)	Oxygen concentration (%)	Power (W)	Temperature (°C)	Film thickness (nm)
ITO	36	–	50	200	165
NiO	35	–	75	RT	140/480
Ta_2O_5	40	–	75	RT	215
W	20	12.5	40	RT	360
ITO	36	–	50	RT	175

RT = Room Temperature.

was maintained at 40 W. Then the Ta_2O_5 films were deposited on the structure of WO_3/ITO/glass. Afterwards, Ta_2O_5/WO_3/ITO/glass structure was exposed to the wet lithiation process. It was investigated that the EC performance of the all-solid-state device were significantly improved with this additional process. The process is given in detail in our previous studies [45–47]. Li^+ ions were injected by the electrochemical cycling into the structure by applying a voltage of 2.5 V in a 0.01 M $LiClO_4$/PC electrolyte solution. Then, the structure was cleaned and dried with Ar gas and was placed into the vacuum chamber to deposit the NiO as an anodic layer and the ITO as a top contact electrode. The deposition parameters of each layer were given in Table 4. Finally, the devices were sealed with transparent epoxy resin to prevent the absorption of moisture in the atmosphere. The only difference between these two devices was the thickness of the NiO film while the main device configuration kept same.

The optical transmission of the as-deposited all-solid-state ECD-1 and ECD-2 were 84.2% and 68.5% at 550 nm, respectively. The optical transmission spectra for the colored and bleached states of the devices

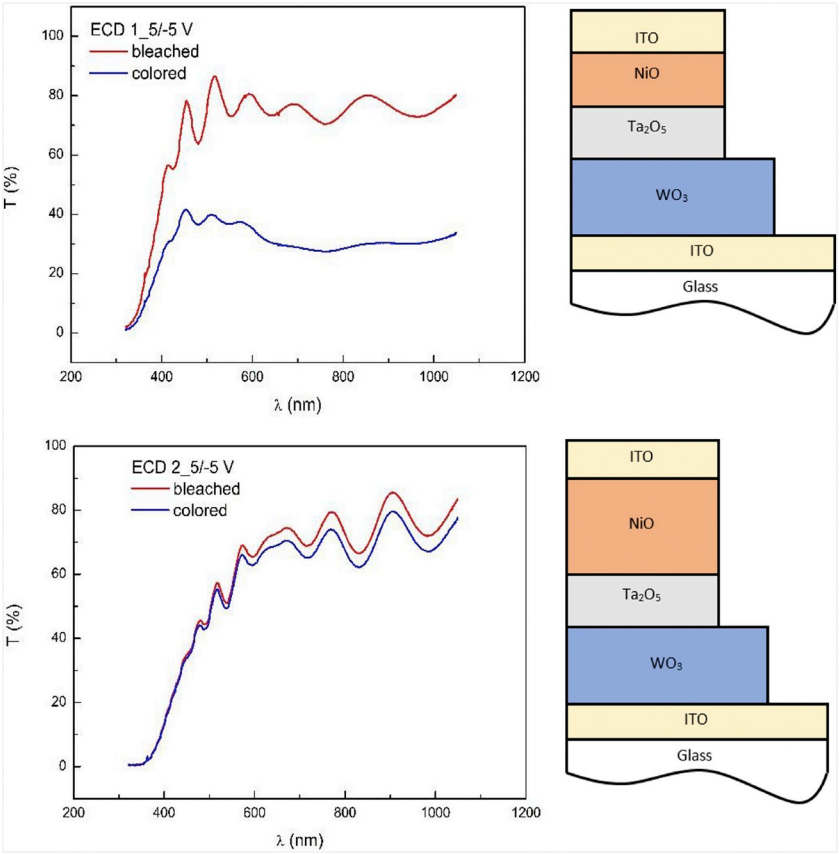

Fig. 12. Optical transmission spectra for the colored and bleached states of the devices at a voltage of ± 5 V for a) ECD-1, b) ECD-2.

at a voltage of ± 5 V were given in Fig. 12. The ECD-1 device, which has thick NiO layer, has a higher optical modulation compared to the ECD-2. The optical modulation of the ECD-1 and ECD-2 were found to be 36.4% (from a colored state of 36.7% to a bleached state of 73.1%) and 1.5% (from a colored state of 54.4% to a bleached state of 55.9%) at 550 nm, respectively. The results indicated the importance of the thickness of the individual EC layer in the overall performance of the EC device. In general, ECDs have been fabricated by the sequential deposition of the layer with individually best EC properties. However, in the current study, it is investigated that the device with the thickest anodic layer having a lower EC performance compared to the thinnest one having better overall EC performance. The results in this study describe a new approach for designing and fabricating of the all-solid-state ECDs with enhanced performance.

4. Conclusion

The optical, structural and electrochromic properties of the NiO films with various thicknesses, which were deposited by using the RF magnetron sputtering technique, were investigated in detail. It was observed that the optical transmission decreased with the increase of film thickness. The coloration efficiency and optical modulation of the films increased with increasing film thickness. The highest coloration efficiency and optical modulation were obtained for the NiO film with a thickness of 480 nm. The highest diffusion rate and ionic conductivity were also obtained for the NiO film with a thickness of 480 nm.

Two all-solid-state electrochromic devices were fabricated by using the NiO results. The thickest NiO film had a high coloration efficiency in the half-cell configuration. On the other hand, it is observed that the thinnest NiO film was more suitable for the fabrication of the device. In addition, when no voltage is applied, a lower transmission was found in the as-deposited device with a thick NiO layer. Therefore, a thicker NiO film performs a better electrochromic performance in a half-cell configuration, while electrochromic device fabrication with a complete-cell configuration could be done with a thinner layer of NiO.

Acknowledgements

This work is partially supported by The Scientific and Technological Research Council of Turkey (TÜBİTAK) under the grant number of 111T252 and by Hacettepe University Research Projects Management System under the grant number of FDK-2017-13852.

The authors are grateful to The Scientific and Technological Research Council for contributing our research with 2014/1 2211-C Domestic Priority Areas for Doctoral Scholarship Program.

References

[1] E. Turgut, Ö. Çoban, S. Sarıtaş, S. Tüzemen, M. Yıldırım, E. Gür, Oxygen partial pressure effects on the RF sputtered p-type NiO hydrogen gas sensors, Appl. Surf. Sci. 435 (2018) 880–885, https://doi.org/10.1016/j.apsusc.2017.11.133.

[2] A.A. Ahmed, M. Devarajan, N. Afzal, Effects of substrate temperature on the degradation of RF sputtered NiO properties, Mater. Sci. Semicond. Process. 63 (2017) 137–141, https://doi.org/10.1016/j.mssp.2017.02.017.

[3] X. Yan, J. Zheng, L. Zheng, G. Lin, H. Lin, G. Chen, B. Du, F. Zhang, Optimization of sputtering NiO_x films for perovskite solar cell applications, Mater. Res. Bull. 103 (2018) 150–157, https://doi.org/10.1016/j.materresbull.2018.03.027.

[4] G. Atak, Ö. Duyar Coşkun, Annealing effects of NiO thin films for all-solid-state electrochromic devices, Solid State Ionics 305 (2017) 43–51, https://doi.org/10.1016/j.ssi.2017.05.002.

[5] Y. Zhao, H. Wang, X. Gong, J. Wang, H. li, M. Tang, X. Li, Effect of lithium-ion doping concentration on structural and optical properties of NiO films fabricated by magnetron sputtering, Vacuum 137 (2017) 56–59, https://doi.org/10.1016/j.vacuum.2016.12.027.

[6] J.D. Hwang, T.H. Ho, Effects of oxygen content on the structural, optical, and electrical properties of NiO films fabricated by radio-frequency magnetron sputtering, Mater. Sci. Semicond. Process. 71 (2017) 396–400, https://doi.org/10.1016/j.mssp.2017.09.002.

[7] A. Singh, S. Bhansali, D. Barton, F.K. Urban III, Reactive sputter deposition and

annealing of nanometer scale NiO thin films for metal-insulator-metal tunnel junction diodes, Thin Solid Films 644 (2017) 23–28, https://doi.org/10.1016/j.tsf.2017.06.063.
[8] Y. Zhao, H. Wang, F. Yang, Z. Zhen, X. Li, Q. Li, J. Li, Influence of growth temperature on structure, optical and electrical properties of nickel oxide films by magnetron sputtering, Vacuum 151 (2018) 163–166, https://doi.org/10.1016/j.vacuum.2018.02.026.
[9] H.-L. Chen, Y.-M. Lu, W.-S. Hwang, Thickness dependence of electrical and optical properties of sputtered nickel oxide films, Thin Solid Films 498 (2006) 266–270, https://doi.org/10.1016/j.tsf.2005.07.124.
[10] K.D. Lee, W.C. Jung, Effect of substrate temperature on the electrochromic properties and cyclic durability of nickel oxide films, J. Korean Phys. Soc. 45 (2004) 447–454.
[11] T.M. Roffi, S. Nozaki, K. Uchida, Growth mechanism of single-crystalline NiO thin films grown by metal organic chemical vapor deposition, J. Cryst. Growth 451 (2016) 57–64, https://doi.org/10.1016/j.jcrysgro.2016.06.047.
[12] K.K. Purushothaman, G. Muralidharan, Nanostructured NiO based all solid-state electrochromic device, J. Sol-Gel Sci. Technol. 46 (2008) 190–194, https://doi.org/10.1007/s10971-007-1657-0.
[13] Q. Liu, Q. Chen, Q. Zhang, G. Dong, X. Zhong, Y. Xiao, M.-P. Selplancke-Ogletree, F. Reniers, X. Diao, Dynamic behaviors of inorganic all-solid-state electrochromic device: role of potential, Electrochim. Acta 269 (2018) 617–623, https://doi.org/10.1016/j.electacta.2018.02.050.
[14] Y. Xiao, X. Zhong, J. Guo, C. Zhou, H. Zuo, Q. Liu, Q. Huang, Q. Zhang, X. Diao, The role of interface between LiPON solid electrolyte and electrode in inorganic monolithic electrochromic devices, Electrochim. Acta 260 (2018) 254–263, https://doi.org/10.1016/j.electacta.2017.12.020.
[15] Y. Xiao, G. Dong, J. Guo, Q. Liu, Q. Huang, Q. Zhang, X. Zhong, X. Diao, Thickness dependent surface roughness of sputtered $Li_{2.5}TaO_x$ ion conductor and its effect on electro-optical performance of inorganic monolithic electrochromic device, Sol. Energy Mater. Sol. Cells 179 (2018) 319–327, https://doi.org/10.1016/j.solmat.2017.12.027.
[16] A. Mallikarjuna Reddy, A. Sivasankar Reddy, P. Sreedhara Reddy, Thickness dependent properties of nickel oxide thin films deposited by dc reactive magnetron sputtering, Vacuum 85 (2011) 949–954, https://doi.org/10.1016/j.vacuum.2011.02.002.
[17] M.D. Rocha, Y. He, X. Diao, A. Rougier, Influence of cycling temperature on the electrochromic properties of WO3//NiO devices built with various thicknesses, Sol. Energy Mater. Sol. Cells 177 (2018) 57–65, https://doi.org/10.1016/j.solmat.2017.05.070.
[18] D.R. Sahu, T.-J. Wu, S.-C. Wang, J.-L. Huang, Electrochromic behavior of NiO film prepared by e-beam evaporation, Journal of Science: Advanced Materials and Devices 2 (2017) 225–232, https://doi.org/10.1016/j.jsamd.2017.05.001.
[19] V. Gupta, A. Mansingh, Influence of postdeposition annealing on the structural and optical properties of sputtered zinc oxide film, J. Appl. Phys. 80 (2) (1996) 1063–1073, https://doi.org/10.1063/1.362842 July.
[20] K. Nadarajah, C.Y. Chee, C.Y. Tan, Influence of annealing on properties of spray deposited ZnO thin films, J. Nanomater. (2013), https://doi.org/10.1155/2013/146382 (Article ID 146382 8 pages).
[21] Ö. Duyar Coşkun, S. Demirel, G. Atak, The effects of heat treatment on optical, structural, electrochromic and bonding properties of Nb_2O_5 thin films, J. Alloys Compd. 648 (2015) 994–1004, https://doi.org/10.1016/j.jallcom.2015.07.053.
[22] R.K. Kawar, P.S. Chigare, P.S. Patil, Substrate temperature dependent structural, optical and electrical properties of spray deposited iridium oxide thin films, Appl. Surf. Sci. 206 (2003) 90–101, https://doi.org/10.1016/S0169-4332(02)01191-1.
[23] A. Sawaby, M.S. Selim, S.Y. Marzouk, M.A. Mostafa, A. Hosny, Structure, optical and electrochromic properties of NiO thin films, Physica B 405 (2010) 3412–3420, https://doi.org/10.1016/j.physb.2010.05.015.
[24] Y. Akaltun, T. Çayır, Fabrication and characterization of NiO thin films prepared by SILAR method, J. Alloys Compd. 625 (2015) 144–148, https://doi.org/10.1016/j.jallcom.2014.10.194.
[25] K.S. Usha, R. Sivakumar, C. Sanjeeviraja, Optical constants and dispersion energy parameters of NiO thin films prepared by radio frequency magnetron sputtering technique, J. Appl. Phys. 114 (2013) 123501, , https://doi.org/10.1063/1.4821966.
[26] D.S. Dalavi, M.J. Suryavanshi, D.S. Patil, S.S. Mali, A.V. Moholkar, S.S. Kalagi, S.A. Vanalkar, S.R. Kang, J.H. Kim, P.S. Patil, Nanoporous nickel oxide thin films and its improved electrochromic performance: effect of thickness, Appl. Surf. Sci. 257 (2011) 2647–2656, https://doi.org/10.1016/j.apsusc.2010.10.037.
[27] M.M. Uplane, S.H. Mujawar, A.I. Inamdar, P.S. Shinde, A.C. Sonavane, P.S. Patil, Structural, optical and electrochromic properties of nickel oxide thin films grown from electrodeposited nickel sulphide, Appl. Surf. Sci. 253 (2007) 9365–9371, https://doi.org/10.1016/j.apsusc.2007.05.069.
[28] F.I. Ezema, A.B.C. Ekwealor, R.U. Osuji, Optical properties of chemical bath deposited nickel oxide (NiO_x) thin films, Superficies Y Vacío 21 (1) (2008) 6–10.
[29] A.E. Jimenez-Gonzalez, J.G. Cambray, Deposition of NiO_x thin films by sol–gel technique, Surf. Eng. 16 (1) (2000) 73–76, https://doi.org/10.1179/026708400322911573.
[30] K.N. Manjunatha, S. Paul, Investigation of optical properties of nickel oxide thin films deposited on different substrates, Appl. Surf. Sci. 352 (2015) 10–15, https://doi.org/10.1016/j.apsusc.2015.03.092.
[31] F. Lai, M. Li, H. Wang, H. Hu, X. Wang, J.G. Hou, Y. Song, Y. Jiang, Optical scattering characteristic of annealed niobium oxide films, effect of thickness on the structure, morphology and optical properties of sputter deposited Nb_2O_5 films, Thin Solid Films 488 (2005) 314320, https://doi.org/10.1016/j.tsf.2005.04.036.
[32] J.-H. Lee, B.-W. Yeo, B.-O. Park, Effects of the annealing treatment on electrical and optical properties of ZnO transparent conduction films by ultrasonic spraying pyrolysis, Thin Solid Films 457 (2004) 333–337, https://doi.org/10.1016/j.tsf.2003.09.075.
[33] I. Sta, M. Jlassi, M. Kandyla, M. Hajjia, P. Koralli, R. Allagui, M. Kompitsas, H. Ezzaoui, Hydrogen sensing by sol–gel grown NiO and NiO: Li thin films, J. Alloys Compd. 626 (2015) 87–92, https://doi.org/10.1016/j.jallcom.2014.11.151.
[34] K.-S. Ahn, Y.-C. Nah, Y.-E. Sung, Thickness dependent microstructural and electrochromic properties of sputter-deposited Ni oxide films, J. Vac. Sci. Technol. A 20 (2002) 1468–1474, https://doi.org/10.1116/1.1487871.
[35] Z. Sun, C. Cao, L. Cao, P. Liang, X. Huang, X. Song, Surface morphology and optical properties of magnetron – sputtered ultrathin Al films, Vacuum 84 (2010) 828–832, https://doi.org/10.1016/j.vacuum.2009.11.002.
[36] C.G. Granqvist, Handbook of Inorganic Electrochromic Materials, Elsevier, Amsterdam, 1995.
[37] S. Pereira, A. Gonçalves, N. Correia, J. Pinto, L. Pereira, R. Martins, E. Fortunato, Electrochromic behavior of NiO thin films deposited by e-beam evaporation at room temperature, Sol. Energy Mater. Sol. Cells 120 (2014) 109–115, https://doi.org/10.1016/j.solmat.2013.08.024.
[38] A.C. Sonavane, A.I. Inamdar, P.S. Shinde, H.P. Deshmukh, R.S. Patil, P.S. Patil, Efficient electrochromic nickel oxide thin films by electrodeposition, J. Alloys Compd. 489 (2010) 667–673, https://doi.org/10.1016/j.jallcom.2009.09.146.
[39] G. Leftheriotis, S. Papaefthimiou, P. Yianoulis, Dependence of the estimated diffusion coefficient of Li_xWO_3 films on the scan rate of cyclic voltammetry experiments, Solid State Ionics 178 (2007) 259–263, https://doi.org/10.1016/j.ssi.2006.12.019.
[40] V.V. Kondalkar, P.B. Patil, R.M. Mane, P.S. Patil, S. Choudhury, P.N. Bhosal, Electrochromic performance of nickel oxide thin film: synthesis via electrodeposition technique, Macromol. Symp. 361 (2016) 47–50, https://doi.org/10.1002/masy.201400253.
[41] G.A. Niklasson, C.G. Graqvist, Electrochromics for smart windows: thin films of tungsten oxide and nickel oxide, and devices based on these, J. Mater. Chem. 17 (2007) 127–156, https://doi.org/10.1039/b612174h.
[42] H. Huang, J. Tian, W.K. Zhang, Y.P. Gan, X.Y. Tao, X.H. Xia, J.P. Tu, Electrochromic properties of porous NiO thin film as a counter electrode for NiO/WO_3 complementary electrochromic window, Electrochim. Acta 56 (2011) 4281–4286, https://doi.org/10.1016/j.electacta.2011.01.078.
[43] R.D. Armstrong, H. Wang, Behaviour of nickel hydroxide electrodes after prolonged potential float, Electrochim. Acta 36 (1991) 759–762, https://doi.org/10.1016/0013-4686(91)85271-8.
[44] X. Qian, N. Gu, Z. Cheng, X. Yang, E. Wang, S. Dong, Methods to study the ionic conductivity of polymeric electrolytes using a.c. impedance spectroscopy, J. Solid State Electrochem. 6 (2001) 8–15, https://doi.org/10.1007/s100080000190.
[45] G. Atak, Ö. Duyar Coşkun, Fabrication of an all solid-state electrochromic device using zirconium dioxide as an ion-conducting layer, Thin Solid Films 664 (2018) 70–78, https://doi.org/10.1016/j.tsf.2018.08.030.
[46] G. Atak, Ö. Duyar Coşkun, $LiNbO_3$ thin films for all-solid-state electrochromic devices, Opt. Mater. 82 (2018) 160–167, https://doi.org/10.1016/j.optmat.2018.05.062.
[47] Ö. Duyar Coşkun, G. Atak, The effects of lithiation process on the performance of all-solid-state electrochromic devices, Thin Solid Films 662 (2018) 13–20, https://doi.org/10.1016/j.tsf.2018.07.019.